scientific reports



OPEN

A superior coherent perfect absorber and laser constructed from the periodic ring optical waveguide network based on extremum spontaneous PTsymmetric breaking points

Yao Zhang^{1,2}, Xiangbo Yang^{1,2™} & Mengli Huang^{1,2}

In this study, we propose a superior coherent perfect absorber and laser (CPA laser) constructed from the one-dimensional (1D) two-material (TM) parity-time (PT) symmetric periodic ring optical waveguide network (PROWN). A novel method based on seeking the exact extremum spontaneous PT-symmetric breaking points is used for determining the imaginary part of the refractive indices of the materials composed of waveguides. The minimal overall output coefficient Θ_{\min} and maximal transmissivity T_{\max} can reach 3.1914×10^{-16} and 1.5667×10^{15} , respectively, which are 9 orders of magnitude smaller and larger than the previously reported values, respectively. It is also found that with the increment of unit cells, Θ_{\min} increases monotonically while T_{\max} decreases monotonically. Moreover, Θ_{\min} and T_{\max} are found to be varied with the periodicity of 1.866152 MHz. Our work provides a new method for optimizing CPA lasers.

Keywords Waveguide network, \mathcal{PT} -symmetry, CPA laser

As a new kind of artificial structure for controlling and confining the propagation of electromagnetic (EM) waves, parity-time (PT) symmetric systems have attracted significant attention in recent years^{1–24}. When EM waves propagate in a PT-symmetric system, the coupled gain and loss effects produce many extraordinary optical characteristics. These extraordinary optical characteristics include unidirectional invisibility^{4–9}, anisotropic transmission resonances⁵, ultra-strong transmission and reflection^{5,10,11}, dual behavior of PT-symmetric scattering^{3,6}, and coherent perfect absorbers and lasers (CPA lasers)^{12–21}. CPA lasers are a unique optical structure¹⁴, where two counter-propagating incident signals passing through an optical medium can simultaneously produce lasers while being completely absorbed with the same frequency. CPA lasers may be the potential for designing high-efficiency all-optical switches, sensor light modulators, and transducers¹³.

It is known that many CPA lasers are designed based on PT-symmetric photonic crystals. Longhi 12 developed a CPA laser utilizing a grating photonic crystal structure with a minimal overall output coefficient and the maximal transmissivity of 10^{-4} and 10^3 orders of magnitude, respectively. Wong et al. 16 experimentally construct a CPA laser in a PT-symmetric photonic crystal of 500-nm-thick InGaAsP multiple quantum wells as a gain medium on an InP substrate with the minimal overall output coefficient and the maximal transmissivity of 10^{-1} and 10 orders of magnitude, respectively. Ge and Feng 17 constructed a CPA laser with a one-dimensional (1D) PT-symmetric periodic photonic crystal structure with a minimal overall output coefficient and maximal transmissivity reaching up to 10^{-7} and 10^6 orders of magnitude, respectively.

As another photonic bandgap structure, optical waveguide networks can also realize CPA lasers¹⁹. Recently, we proposed a CPA laser by using a 1D two-material (TM) PT-symmetric (PTS) periodic ring optical waveguide

¹Guangdong Provincial Key Laboratory of Nanophotonic Functional Materials and Devices, School of Information and Optoelectronic Science and Engineering, South China Normal University, Guangzhou 510006, China. ²Longgang Affiliated High School of Central China Normal University, Shenzhen 518116, China. [™]email: xbyang@scnu.edu.cn

network (PROWN) collectively called 1D TMPTSPROWN¹⁹. The minimal overall output coefficient of 1.892×10^{-5} and the maximal transmissivity of 2.981×10^4 were simultaneously obtained for that CPA laser.

It is well known that if there is stronger absorption and more considerable amplification simultaneously, CPA lasers will have better performance. Although our recently proposed CPA laser based on an optical waveguide network has an excellent performance, further improved CPA lasers by a new physical mechanism is desirous.

The new physical mechanism seeks exact extremum spontaneous PT-symmetric breaking points, which can determine the imaginary part of the material's refractive index. Then the intrinsic frequency of the PT-symmetric system can be precisely determined. When EM waves with this frequency transmit through the network, superstrong anti-resonance and resonance effects can be created. Then ultra-efficient anti-lasing and lasing modes can be generated.

Our aforementioned recently work ¹⁹ mainly focused on exploring whether a CPA laser can be implemented in an optical waveguide network and did not care about the optimization of both the structural parameters of the network and the working frequency of EM waves. In this study, based on seeking the exact extremum spontaneous PT-symmetric breaking points²⁵, we determine the best values of the imaginary part of the refractive indices of the materials composed of waveguides and the working frequency of EM waves to optimize the CPA laser. The result shows that the minimal overall output coefficient of the CPA laser is reduced by 11 orders of magnitude and reaches a value of 3.1914×10^{-16} . Similarly, the maximal transmissivity of this optimized CPA laser is increased by 11 orders of magnitude reading a value of 1.5667×10^{15} . This work provides an efficient method for the proposing of CPA lasers based on both photonic crystals and optical waveguide networks.

This paper is organized as follows. "Model and theory" section introduces the model and main theoretical and numerical computational methods. The research results of this work, including the parameters of the extremum spontaneous PT-symmetric breaking points and the extraordinary performance of the CPA laser, are given in "Optimization of PT-symmetric optical waveguide networks and extraordinary CPA laser characteristics" section. Finally, the summary of this paper is given in "Conclusion" section.

Model and theory Optimization of model

In order to study the influence of the new physical mechanism on the performance of the CPA laser and to compare this work with our recently proposed CPA laser¹⁹, we optimize and adjust the recently reported model by the new mechanism and investigate the differences of the absorption and amplification between the two resulting CPA lasers. The model, i.e., the 1D TMPTSPROWN with N unit cells, was used for our recently proposed CPA laser¹⁹ and the CPA laser developed in this work is shown in Fig. 1. For convenience, the input and output ends were set to be vacuum, and the refractive index $n_0 = 1$, as shown by the solid black line in Fig. 1. E_a , E_b , E_c , and E_d represent the left input, left output, right input, and right output EM waves, respectively.

The upper and lower arms in a unit cell are all PT-symmetric optical waveguide segments made of Si_3N_4 material²⁶. The lengths of the blue (loss) and red (gain) sub-segments equal l/2, and their refractive indices are n_1 and n_2 , respectively. The values of n_1 and n_2 are given as follows

$$\begin{cases} n_1 = n_{\text{Si}_3\text{N}_4} + in_{\text{I}}, \\ n_2 = n_{\text{Si}_3\text{N}_4} - in_{\text{I}}. \end{cases}$$
 (1)

Figure 2a illustrates a unit cell where waveguide lines connected to each other by connectors. The ports of the connectors can be used to measure the amplitudes of the EM waves. Figure 2b shows the structure of the waveguide line, which consists of $\mathrm{Si}_3\mathrm{N}_4$ core conductor, a BaSF insulating cladding, a mesh fabric shielding layer, and a polyethylene coating. Figure 2c shows the input and output of electromagnetic waves at nodes. It is worth noting that the red bar portion and the blue bar portion denote the gain medium $(n_1 = n_{\mathrm{Si}_3\mathrm{N}_4^+})$ and loss medium $(n_2 = n_{\mathrm{Si}_3\mathrm{N}_4^-})$, respectively, for the $\mathrm{Si}_3\mathrm{N}_4$ material with the imaginary part of the refractive index as n_I .

It is reported that in the range of 54.5–968 THz with a corresponding wavelength range of 0.31–5.5 μm , the dispersion equation of $\mathrm{Si_3N_4}$ satisfies the following Sellmeier equation²⁷:

$$n_{\rm Si_3N_4}^2(\lambda) = 1 + \frac{3.0249\lambda^2}{\lambda^2 - 0.1353406^2} + \frac{40314\lambda^2}{\lambda^2 - 1239.842^2},\tag{2}$$

where the unit of λ is μm and the dispersion curve is shown in Fig. 3.

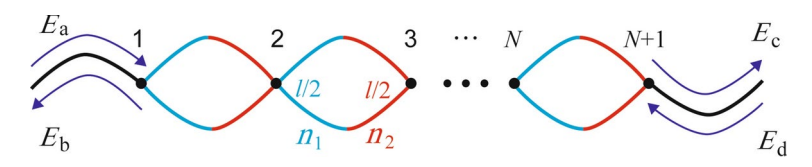


Fig. 1. Schematic diagram of the 1D TMPTSPROWN with N unit cells, where E_a , E_b , E_c , and E_d denote the left input, left output, right input, and right output EM waves, respectively. The solid blue lines are loss subsegments with refractive index n_1 , the solid red lines are gain sub-segments with refractive index n_2 , and the solid black lines are vacuum waveguide segments with refractive index n_0 .

Fig. 2. Waveguide structure diagram. (a) We use connectors to realize the structure of a cell of the model. (b) Materials distributing in transverse section. (c) Materials distributing in radial section.

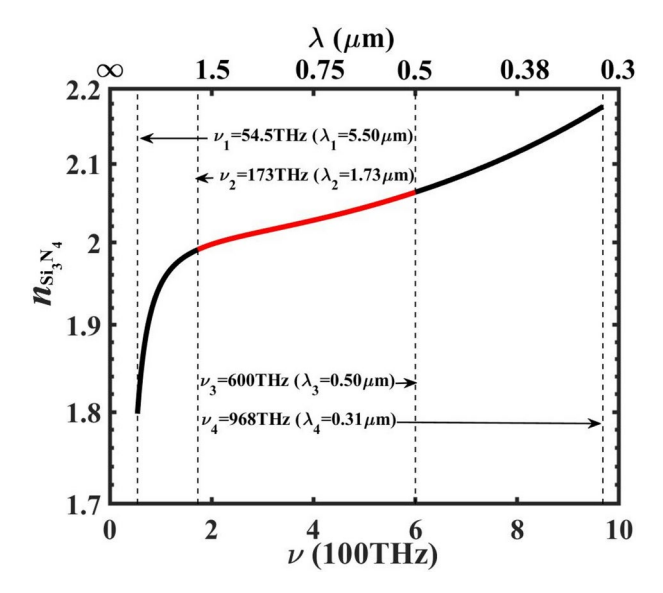


Fig. 3. The dispersion curve of $\mathrm{Si_3N_4}$ defined by Eq. (2). The range of the thick red solid line is investigated in this work. The thin black dashed lines are all scaling lines, and their values are $\nu_1 = 54.5$ THz ($\lambda_1 = 5.50$ μm), $\nu_2 = 173$ THz ($\lambda_2 = 1.73 \mu m$), $\nu_3 = 600$ THz ($\lambda_3 = 0.50 \mu m$), and $\nu_4 = 968$ THz ($\lambda_4 = 0.31 \mu m$).

In order to investigate CPA lasers performance close to the communication wavelength, we only study the EM waves with the frequency (wavelength) in the range of 173–600 THz (0.5–1.73 μm), which corresponds to the part of the dispersion curve with the thick red solid line in Fig. 3.

Compared with our recently proposed the CPA laser reported earlier¹⁹, we have accomplished some optimizations and adjustments with the newly proposed CPA laser in this work. Firstly, the imaginary part of the refractive indices of the waveguide materials is optimized by seeking the exact extremum breaking points. In our previous reported work¹⁹, the refractive indices of the material were set to be 2 and 0.2 for the real and imaginary parts, respectively, for convenience. However, these settings only allow the network to achieve CPA lasers but do not ensure strong resonance effects. In order to improve the resonance efficiency of the PT-symmetric system and consequently reform the CPA laser performance, we determine the imaginary part of the refractive indices of the waveguide materials by seeking the extremum breaking points of the respective PT-symmetric network. Through the method for seeking the extremum breaking points of a PT-symmetric network proposed by our group²⁵, one can obtain the first, second, and third extremum breaking points. Discussion about it is presented in "Extremum spontaneous PT-symmetric breaking points" section. The imaginary parts of the refractive indices of the materials for these three breaking points are $n_{\rm II} = 1.5447 \times 10^{-8}$, $n_{\rm II} = 9.5557 \times 10^{-6}$, and $n_{\rm II} = 2.1837 \times 10^{-8}$.

Secondly, in order to set the working wavelength of the CPA laser close to the communication wavelength of 1.550 μm , the length of the waveguide segment is adjusted in this work. In our previous work 19 , the waveguide length was set as the unit length of value 1 for convenience. However, in this study, the waveguide length is taken as the absolute length for experimental convenience. Based on the discussion in "Extremum spontaneous PT-symmetric breaking points" section, to make our system work with the present optical communication systems, we choose the wavelength of the first extremum breaking point to be the working wavelength $\lambda_{\rm work}$ and adjust this wavelength close to the communication wavelength $\lambda_{\rm comm}=1.550~\mu m$. In other words, $\omega_{\rm work}=2\pi c/\lambda_{\rm work}\approx 2\pi c/\lambda_{\rm comm}\approx 0.5\pi c/l$. Finally, the waveguide length comes out to be $l\approx 0.5\lambda_{\rm comm}/2\approx 0.388~\mu m$.

Two-material network equation

The network equation describes the propagation of EM waves in an optical waveguide network^{25,28,29}. The system in Fig. 1 is a PT-symmetric optical waveguide network, and each waveguide is composed of two materials. Consequently, the two-material network equation calculates the transmissivity, reflectivity, and CPA lasers. In this section, the deduction of the two-material network equation is given as follows

$$-\sum_{i} \psi_{i} \frac{2k_{x}}{\Xi \sin \Pi + \Omega \sin \Lambda} + \psi_{j} \sum_{i} \frac{\Xi \cos \Pi + \Omega \cos \Lambda}{\Xi \sin \Pi + \Omega \sin \Lambda} = 0,$$
(3)

where,

$$\begin{cases}
\Xi = k_x + k_y, \\
\Omega = k_x - k_y, \\
\Pi = \frac{1}{2}(k_x + k_y), \\
\Lambda = \frac{1}{2}(k_y - k_x).
\end{cases} \tag{4}$$

It is important to note that in all waveguides connected to the node j, k_y is the wave vector of the sub-segment for the waveguide directly connected to the node j and k_x is the wave vector corresponding to the waveguide that is not directly connected to the node j. Moreover, ψ_i and ψ_j are the wave functions at the node j and node i.

Generalized eigenfunction method

The generalized eigenfunction method The generalized eigenfunction method is a commonly used method to solve the network transmission and reflection coefficient 28,30. This method regards the network transmission and reflection coefficient as a generalized wave function, and then transforms the correlation equations between the wave functions of each node into is a coefficient matrix, and the transmission-reflection coefficient of the network can be obtained by solving the eigenvalues of the coefficient matrix. This paper uses the generalized eigenfunction method to solve the transmission coefficient of the single unit cell network and the reflection coefficient at left incident and right incident.

Transfer matrix method

The transmission matrix method is a convenient method to solve the transmission and reflection coefficient of electromagnetic waves when they propagate in finite period systems. For a PT symmetric single unit-cell system, the transfer matrix M_1 is given as follows³¹:

$$\mathbf{M}_{1} = \begin{pmatrix} m_{11} & m_{12} \\ m_{21} & m_{22} \end{pmatrix} = \begin{pmatrix} \frac{1}{t_{1}^{*}} & \frac{r_{1-R}}{t_{1}} \\ -\frac{r_{1-L}}{t_{1}} & \frac{1}{t_{1}} \end{pmatrix}, \tag{5}$$

where t_1 , r_{1-L} , and r_{1-R} the transmission, the left and right reflection coefficients of the single unit cell system, respectively.

Similarly, the transfer matrix M_N of an N-unit cell system is

$$\mathbf{M}_{N} = \begin{pmatrix} M_{11} & M_{12} \\ M_{21} & M_{22} \end{pmatrix} = \begin{pmatrix} \frac{1}{t_{N}^{*}} & \frac{r_{N-R}}{t_{N}} \\ -\frac{r_{N-L}}{t_{N}} & \frac{1}{t_{N}} \end{pmatrix}, \tag{6}$$

where t_N , r_{N-L} , and r_{N-R} are the transmission, the left and right reflection coefficients of the N unit cell system, respectively. Since the transfer matrix of all unit cells is identical in our model, the transfer matrix \mathbf{M}_N can be written as the Nth power of \mathbf{M}_1^{31} . One can obtain the transfer matrix \mathbf{M}_N from Eq. (5) and the Chebyshev identity³².

$$\mathbf{M}_{N} = \begin{pmatrix} \frac{1}{t_{1}^{*}} \frac{\sin N\phi - \sin(N-1)\phi}{\sin \phi} & \frac{r_{1-R}\sin N\phi}{t_{1}\sin \phi} \\ -\frac{r_{1-L}\sin N\phi}{t_{1}\sin \phi} & \frac{1}{t_{1}} \frac{\sin N\phi - \sin(N-1)\phi}{\sin \phi} \end{pmatrix},$$
(7)

where ϕ is the Bloch phase, i.e., the phase of the two eigenvalues $\lambda_{1,2}=e^{\pm i\phi}$ of \mathbf{M}_1^{29} , and satisfies the following equation:

$$\cos \phi = \frac{1}{2} \left(\lambda_1 + \lambda_2 \right) = \operatorname{Re} \frac{1}{t_1}. \tag{8}$$

At the same time, the study shows that the theoretical derivation of optical waveguide network to calculate transmittance and reflectivity through transmission matrix can be verified by experiments³³.

Generalized Floquet-Bloch theorem

Bloch's theorem is well-established for analyzing the energy band structure of electrons in materials with periodic potential fields. In the network proposed in this paper, however, the waveguide lines can be bent freely. This design lacks spatial translation periodicity and instead exhibits only topological translation periodicity.

Given this unique characteristic, we can apply the dimensionless generalized Bloch theorem^{29,34}, to determine the dispersion relationship of photons within these topologically periodic structures:

$$\psi_{K}(N+T) = \psi_{K}(N) e^{iK \cdot T}, \tag{9}$$

where K, N and T are dimensionless Bloch wave vectors, node labeling vectors and structural translation vectors, respectively. One can define the photonic propagation modes, deduce the dispersion relation of the network, and determine the distribution of the photonic modes using the generalized Floquet–Bloch theorem. For the 1D TMPTSPROWN, based on the generalized Floquet–Bloch theorem and the two-material network equation, one can gain the dispersion relation as

$$\cos K = f(\nu), \tag{10}$$

where the dispersion function is given as

$$f(\nu) = \frac{\left(\sum_{i} \frac{\Xi \cos \Pi + \Omega \cos \Lambda}{\Xi \sin \Pi + \Omega \sin \Lambda}\right)}{\left(\sum_{i} \frac{2k_{x}}{\Xi \sin \Pi + \Omega \sin \Lambda}\right)}.$$
(11)

A recent study of our group²⁵ has revealed that $|f(\nu)|=1$ can be regarded as a crucial point for determining the photonic modes in PT-symmetric optical waveguide networks. When $|f(\nu)| \leq 1$, one can infer from Eqs. (10) and (11) that $\operatorname{Im}(\mathbf{K})$ may be very small, and the extraordinary transmission with T>1 cannot be produced. $\operatorname{Im}(\mathbf{K})$ can be exceptionally large only when $|f(\nu)|$ is large enough and extraordinary transmission T>1 can be achieved. Consequently, in the PT-symmetric optical waveguide networks, we defined the photonic modes corresponding to $|f(\nu)| \leq 1$ as weak propagation modes (WPMs) and the photonic modes corresponding to $|f(\nu)| > 1$ as strong propagation modes (SPMs). Under this condition, spontaneous PT-symmetric breaking points are the demarcation points between the weak and strong propagation modes, i.e., the imaginary part of the refractive index $n_{\rm L}$ is located between the WPM and SPM.

Optimization of PT-symmetric optical waveguide networks and extraordinary CPA laser characteristics

Photonic mode distribution

Based on the definition of spontaneous PT-symmetric breaking points, our group has made several attempts $^{25,35-38}$ to show that the optical performance of the system are not prominent at the general spontaneous PT-symmetric breaking points. The optical performance of the system are prominent only at the extremum spontaneous PT-symmetric breaking points, where the dispersion relation f(v) is continuous but not differentiable 25 .

In order to investigate the performance of the CPA laser developed by the 1D PTSPROWN, we numerically calculate the distribution of the photonic modes of this PT-symmetric network. The corresponding results are presented in Fig. 4, where the white and red areas represent WPM and SPM, i.e., weak propagation mode and strong propagation mode, respectively.

One can then seek and determine the extremum breaking points of the network using the distribution diagram of photonic modes given in "Extremum spontaneous PT-symmetric breaking points" section.

Extremum spontaneous PT-symmetric breaking points

Figure 4 shows that in the specified frequency range from 173 to 600 THz, three extremum breaking points of our proposed model can be obtained, which are as follows,

$$\begin{cases}
\nu_1 = 193.522877689455 & \text{THz}, \ n_{\text{I1}} = 1.5447 \times 10^{-8}; \\
\nu_2 = 381.534528290694 & \text{THz}, \ n_{\text{I2}} = 9.5557 \times 10^{-6}; \\
\nu_3 = 563.723496478564 & \text{THz}, \ n_{\text{I3}} = 2.1837 \times 10^{-8}.
\end{cases}$$
(12)

The fault tolerance of our proposed system is remarkably high. Although ν and $n_{\rm I}$ cannot reach such high accuracy and the number of significant digits of ν and $n_{\rm I}$ is reduced, the optical waveguide network still produces CPA lasers with ultra-high efficiency.

For the proposed system to work with the optical communication system, we choose the wavelength of the first extremum breaking point to be the working wavelength $\lambda_{\rm work}$ and adjust this wavelength close to the communication wavelength $\lambda_{\rm comm}$. The length of the waveguide is 0.388 μm . Consequently, the length of the waveguide and the material's refractive index are entirely determined. Thus, a greatly optimized optical waveguide network is present, which creates the extraordinary CPA laser performance described in the following two sections.

Ultrastrong CPA laser

The CPA laser can be described by the overall output coefficient Θ , which is the ratio of the total intensity of the outgoing waves to the total intensity of the incident waves of the system³⁹,

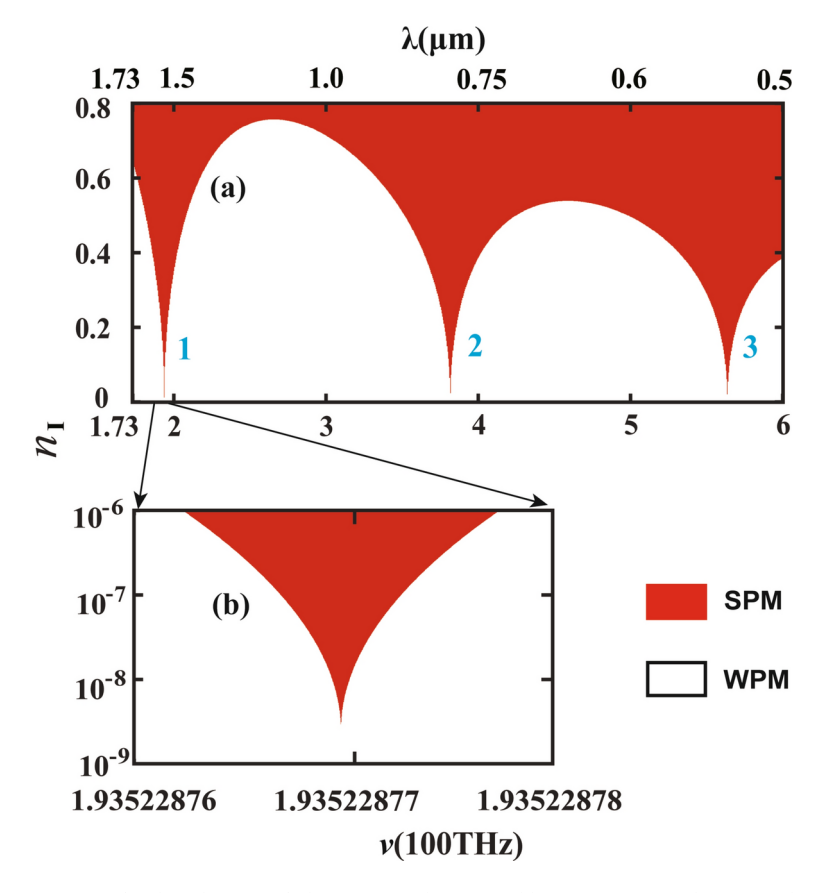


Fig. 4. The distribution of photonic modes created by EM waves in the network presented in Fig. 1. The white and red zones represent WPM and SPM, i.e., weak propagation mode and strong propagation mode, respectively. (a) Frequency range corresponding to the thick red solid line in Fig. 3. (b) Enlarged drawing of the first extremum breaking point.

$$\Theta = \frac{|E_b|^2 + |E_c|^2}{|E_a|^2 + |E_d|^2} = \frac{|1 + \sigma M_{12}|^2 + |\sigma - M_{21}|^2}{\left(1 + |\sigma|^2\right)|M_{22}|^2},\tag{13}$$

where $\sigma=E_d/E_a$ is the ratio of the signals, incident on the left and right sides. CPA lasers need to satisfy the convergence of Θ to 0. Thus, $\sigma=M_{21}$ is one of the sufficient conditions for CPA lasers. Therefore,

$$\Theta = \frac{|1 + M_{21}M_{12}|^2}{\left(1 + |M_{21}|^2\right)|M_{22}|^2}.$$
(14)

It is well known that for an N unit cell system, the following two sufficient conditions together give the perfect state of a CPA laser^{18,19}:

$$\operatorname{Im} \frac{1}{t_1} = 0, \tag{15}$$

$$\sin^2 N\phi = 1. \tag{16}$$

From Eqs. (15) and (16), one can see that the CPA laser highly depends on the number of unit cells and the frequency EM waves.

Our recent studies $^{25,35-38}$ on PT-symmetric optical waveguide networks have revealed that optimizing the network structure parameters by seeking the extremum breaking points can lead to extraordinary ultra-strong transmission, reflection, and photonic localization. In this work, we also found that these optimized systems also create perfect absorption and extremely large amplification. Figure 5 shows the overall output coefficient and transmissivity curves when EM waves transmit through the 1D TMPTSPROWN with a unit cell optimized by three extremum breaking points. The red and blue lines indicate the overall output coefficient Θ and the transmissivity T, respectively. The following two rules can be deduced from the data shown in Fig. 5 and Table 1.

Rule 1: EM waves transmitted through the aforementioned optimized systems can create CPA lasers with high efficiency. The primary reason is that seeking extremum breaking points can precisely determine the intrinsic

Fig. 5. The spectra of the overall output coefficient Θ and transmissivity T of the 1D TMPTSPROWN with a single unit cell optimized by the first-three extremum spontaneous PT-symmetric breaking points. The red and blue solid curves indicate the results of Θ and T, respectively. (a) The first extremum breaking point. (b) The second extremum breaking point. (c) The third extremum breaking point.

Systems	Θ_{\min}	$T_{ m max}$
Determined by $n_{\rm I1}=1.5447\times 10^{-8}$	3.1914×10^{-16}	1.5667×10^{15}
Determined by $n_{\rm I2} = 9.5557 \times 10^{-6}$	4.1493×10^{-14}	1.2053×10^{13}
Determined by $n_{\mathrm{I3}} = 2.1837 \times 10^{-8}$	4.7413×10^{-16}	1.0546×10^{15}
Determined by $n_{\rm Imag}=0.2$	0.8395	1.0428

Table 1. Comparison of Θ_{\min} and T_{\max} of different single-unit cell systems.

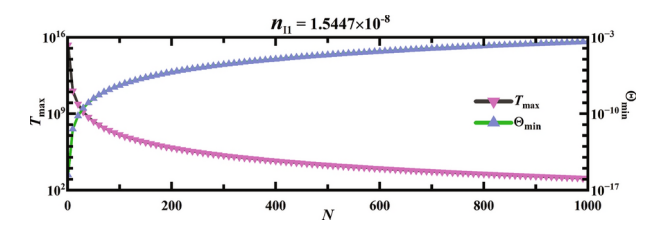


Fig. 6. The variation of Θ_{\min} and T_{\max} versus the number of unit cells N.

frequency of the PT-symmetric system. The EM waves with this frequency will result in super-strong anti-resonance and resonance effects in this network, which correspond to anti-lasing and lasing modes, respectively. The data in Table 1 shows that after optimizing the network structure by the first extremum breaking point, the values of Θ_{\min} and T_{\max} reach up to 3.1914×10^{-16} and 1.5667×10^{15} , respectively. These values of the Θ_{\min} and T_{\max} are 15 orders of magnitude smaller and greater than our previously reported values of Θ_{\min} and T_{\max} , respectively.

Rule 2: The values of Θ_{\min} and T_{\max} produced by the aforementioned optimized systems are at the same frequency. This frequency is the working frequency of the CPA laser corresponding to the single unit system determined by extremum breaking points. The primary reason is that the PT-symmetric system possesses two modes of anti-lasing and lasing for each intrinsic frequency. Consequently, super-strong anti-resonance and resonance effects can be generated in this network at this frequency.

Hence, based on these rules, our proposed CPA laser possess immense potential to become a general-purpose module for next-generation photonic integrated circuits. Moreover, our proposed CPA laser will significantly reduce the integration complexity while enabling versatile operations for efficient information processing in optical communications.

Dependence of CPA laser on unit cell number and frequency

It is well known that the number of unit cells and the frequency for a finite system seriously influence the CPA lasers' characteristics. Therefore, in this section, we numerically investigate the dependence of CPA laser on unit cell number and frequency.

Firstly, for the dependence of the CPA laser on unit cell number, as an example, we develop a CPA laser from a system after determining the first extremum breaking point, and the results are shown in Fig. 6. From Fig. 6, it can be seen that with the increment of the number of unit cells, Θ_{\min} increases monotonically and converges infinitely to 0.1. Similarly, T_{\max} decreases monotonically and converges infinitely to 10. It is because, for a large number of unit cells of the systems, there is a large number of waveguides at the same time. So, the loss and absorption will increase when EM waves transmit through the network. The lasing mode will be weakened while the anti-lasing mode will be enhanced, and it leads to a monotonic decrease in T_{\max} and a monotonic increase in

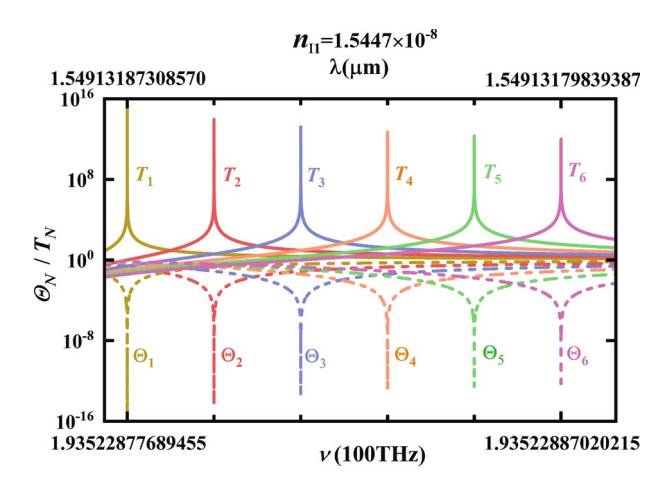


Fig. 7. The spectra of the overall output coefficient Θ and transmissivity T of the 1D TMPTSPROWN optimized by the first extremum breaking point. The subscripts of Θ and T are N, i.e., the number of unit cells.

NO.	Θ_{\min}	$T_{ m max}$	u (THz)
1	3.1914×10^{-16}	1.5667×10^{15}	193.522877689455
2	5.6886×10^{-15}	8.7895×10^{13}	193.522879555607
3	3.0456×10^{-14}	1.6417×10^{13}	193.522881421759
4	9.9347×10^{-14}	5.0329×10^{12}	193.522883287911
5	2.4520×10^{-13}	2.0391×10^{12}	193.522885154063
6	5.0395×10^{-13}	9.9217×10^{11}	193.522887020215

Table 2. Comparison of Θ_{\min} , T_{\max} , and ν , which are for the systems optimized by the first extremum breaking point with N as the number of unit cells.

 Θ_{\min} . Similarly, for systems determined by other extremum breaking points, such as extremum breaking points 2 and 3, a similar rule exists, i.e., as the number of unit cells increases, Θ_{\min} increases monotonically and infinitely converges to 0.1. In contrast, T_{\max} decreases monotonically and infinitely converges to 10.

Secondly, for the dependence of the CPA laser on frequency, as an example, we develop a CPA laser from a system after determining the first extremum breaking point, and the results are shown in Fig. 7. From Fig. 7 and Table 2, one can get the following equation:

$$\nu_N = \nu_1 + (N - 1) \cdot \Delta \nu,\tag{17}$$

where,

$$\begin{cases} \nu_1 = 1.93522877689455 \text{ THz} \\ \Delta \nu = 1.866152 \text{ MHz} \end{cases}$$
 (18)

It can be seen from Eqs. (17) and (18) that with the increment of the number of unit cells, the frequency of Θ_{\min} and T_{\max} increase with the same periodicity of 1.866152 MHz. It means the intrinsic frequency of systems increases with the same periodicity of 1.866152 MHz. It is because, with the increase in the number of unit cells in the network, the system gets large, and correspondingly the intrinsic frequency increase periodically. Similarly, a similar rule exists for systems determined by other extremum breaking points, such as extremum breaking points 2 and 3, i.e., the intrinsic frequency of systems increase periodically with the increase in the number of unit cells.

To evaluate the robustness of the CPA laser's switching mechanism, we introduced a random function to adjust the error Δd for each waveguide segment length, maintaining Δd at a minimal level. Our stochastic analysis yielded the following key findings: (i) Parameters Θ_{\min} and T_{\max} remained stable and consistently displayed ultra-low and ultra-high values, respectively. (ii) The operating frequency of the CPA laser corresponding to the unitary system determined by the extreme breakpoints is correlated with and somewhat influenced by the average error Δd . (iii) As the number of cells increases, Θ_{\min} still converges to 0.1. Correspondingly, T_{\max} converges to 10. The influence of Δd is not obvious; (iv) Since the Θ_{\min} / T_{\max} periodic purple shift frequency value generated by the system's natural frequency is related to Δd , it is significantly affected. These rules provide a theoretical criterion for developing appropriate and optimal CPA laser for PT-symmetric optical waveguide networks at the specified wavelengths with particular operational requirements.

Conclusion

Based on one of our previous studies, in this work, we propose a superior CPA laser constructed from the 1D TMPTSPROWN. A novel method based on seeking the exact extremum spontaneous PT-symmetric breaking points is used for determining the imaginary part of the refractive indices of the materials composed of waveguides. Furthermore, in order to make the working wavelength of the proposed CPA lasers work with practical applications and optical communication systems, we use a suitable waveguide material, $\mathrm{Si}_3\mathrm{N}_4$, adjust the length of the optical waveguides, and set the working wavelength close to the communication wavelength.

Firstly, in order to facilitate experimental verification, the waveguide length of the system is adjusted by seeking extremum breaking points of the PT-symmetric network, i.e., the working wavelength close to the breaking points is set as the communication wavelength. Then the imaginary part of the breaking points is set as the imaginary part of the waveguide material to optimize the refractive indices of the materials.

Secondly, the performance of the CPA lasers created by the optimized PT-symmetric system is investigated based on our previously reported work. It is shown that (i) these systems can produce perfect absorption and substantial amplification, with the best performance of the CPA laser for a single unit-cell system optimized by the first extremum breaking point. The Θ_{\min} reached up to 3.1914×10^{-16} , 9 orders of magnitude smaller than previously reported results of the CPA laser. Moreover, T_{\max} reached a value of 1.5667×10^{15} , which is 9 orders of magnitude larger than previously reported results of the CPA laser. (ii) The values of Θ_{\min} and T_{\max} produced by the aforementioned optimized systems are at the same frequency. This frequency is the working frequency of the CPA lasers corresponding to the single unit system determined by extremum breaking points. (iii) The performance of CPA lasers depends on the number of unit cells in the system. With the increment of the number of unit cells, Θ_{\min} increases monotonically and converges infinitely to 0.1. Correspondingly, T_{\max} decreases monotonically and converges infinitely to 10. (iv) The performance of the CPA laser also depends on the system's frequency. With the increment of the number of unit cells, the frequencies of Θ_{\min} and T_{\max} increase with a periodicity of 1.866152 MHz. These characteristics provide a scientific basis for selecting the most appropriate and optimal CPA lasers for PT-symmetric optical waveguide networks at the specified wavelengths for various operational requirements.

In conclusion, this work provides a new method for optimizing the CPA lasers and optimizing the structure and performance of optical waveguide networks.

Data availability

The data that support the findings of this study are available from the corresponding author upon reasonable request.

Received: 6 May 2024; Accepted: 4 November 2024

Published online: 18 November 2024

References

- El-Ganainy, R., Makris, K. G., Christodoulides, D. N. & Musslimani, Z. H. Theory of coupled optical PT-symmetric structures. Opt. Lett. 32, 2632–2634. https://doi.org/10.1364/OL.32.002632 (2007).
- Musslimani, Z. H., Makris, K. G., El-Ganainy, R. & Christodoulides, D. N. Optical solitons in PT periodic potentials. Phys. Rev. Lett. 100, 030402. https://doi.org/10.1103/PhysRevLett.100.030402 (2008).
- Makris, K. G., El-Ganainy, R., Christodoulides, D. & Musslimani, Z. H. Beam dynamics in PT-symmetric optical lattices. Phys. Rev. Lett. 100, 103904. https://doi.org/10.1103/PhysRevLett.100.103904 (2008).
- Lin, Z. et al. Unidirectional invisibility induced by PT-symmetric periodic structures. Phys. Rev. Lett. 106, 213901. https://doi.org/10.1103/PhysRevLett.106.213901 (2011).
- Ge, L., Chong, Y. D. & Stone, A. D. Conservation relations and anisotropic transmission resonances in one-dimensional PTsymmetric photonic heterostructures. *Phys. Rev. A* 85, 023802. https://doi.org/10.1103/PhysRevA.85.023802 (2012).
- Lin, Z., Schindler, J., Ellis, F. M. & Kottos, T. Experimental observation of the dual behavior of PT-symmetric scattering. Phys. Rev. A 85, 050101 (2012).
- 7. Zhu, X. F., Peng, Y. G. & Zhao, D. G. Anisotropic reflection oscillation in periodic multilayer structures of parity-time symmetry. Opt. Express 22, 18401–18411. https://doi.org/10.1364/OE.22.018401 (2014) https://www.ncbi.nlm.nih.gov/pubmed/25089459.
- 8. Fleury, R., Sounas, D. & Alu, A. An invisible acoustic sensor based on parity-time symmetry. *Nat. Commun.* **6**, 5905. https://doi.org/10.1038/ncomms6905 (2015).
- 9. Jin, L., Zhang, X. Z., Zhang, G. & Song, Z. Reciprocal and unidirectional scattering of parity-time symmetric structures. Sci. Rep. 6, 20976. https://doi.org/10.1038/srep20976 (2016).
- Ding, S. L. & Wang, G. P. Extraordinary reflection and transmission with direction dependent wavelength selectivity based on parity-time-symmetric multilayers. J. Appl. Phys. 117, 023104. https://doi.org/10.1063/1.4905319 (2015).
- 11. Cao, P. C. et al. Ultrastrong graphene absorption induced by one-dimensional parity-time symmetric photonic crystal. *IEEE Photon. J.* 9, 1–9. https://doi.org/10.1109/JPHOT.2017.2653621 (2017).
- 12. Longhi, S. PT-symmetric laser absorber. *Phys. Rev. A* 82, 031801. https://doi.org/10.1103/PhysRevA.82.031801 (2010).
- Chong, Y. D., Ge, L., Cao, H. & Stone, A. D. Coherent perfect absorbers: Time-reversed lasers. Phys. Rev. Lett. 105, 053901. https://doi.org/10.1103/PhysRevLett.105.053901 (2010).
- 14. Chong, Y. D., Ge, L. & Stone, A. D. PT-symmetry breaking and laser-absorber modes in optical scattering systems. *Phys. Rev. Lett.* **106**, 093902. https://doi.org/10.1103/PhysRevLett.106.093902 (2011).
- 15. Roger, T. et al. Coherent perfect absorption in deeply subwavelength films in the single-photon regime. *Nat. Commun.* **6**, 7031. https://doi.org/10.1038/ncomms8031 (2015).
- 16. Wong, Z. J. et al. Lasing and anti-lasing in a single cavity. Nat. Photon. 10, 796–801. https://doi.org/10.1038/nphoton.2016.216 (2016).
- 17. Ge, L. & Feng, L. Contrasting eigenvalue and singular-value spectra for lasing and antilasing in a PT-symmetric periodic structure. *Phys. Rev. A* **95**, 013813. https://doi.org/10.1103/PhysRevA.95.013813 (2017).
- 18. Achilleos, V., Auregan, Y. & Pagneux, V. Scattering by finite periodic PT-symmetric structures. *Phys. Rev. Lett.* 119, 243904. https://doi.org/10.1103/PhysRevLett.119.243904 (2017).
- 19. Wu, H. Z. et al. The scattering problem in PT-symmetric periodic structures of 1D two-material waveguide networks. *Ann. Phys.* 531, 1900120. https://doi.org/10.1002/andp.201900120 (2019).

- Sweeney, W. R., Hsu, C. W., Rotter, S. & Stone, A. D. Perfectly absorbing exceptional points and chiral absorbers. *Phys. Rev. Lett.* 122, 093901. https://doi.org/10.1103/PhysRevLett.122.093901 (2019).
- Pichler, K. et al. Random anti-lasing through coherent perfect absorption in a disordered medium. Nature 567, 351–355. https://doi.org/10.1038/s41586-019-0971-3 (2019).
- 22. Farhat, M., Yang, M., Ye, Z. & Chen, P. Pt-symmetric absorber-laser enables electromagnetic sensors with unprecedented sensitivity. ACS Photon. 7, 2080–2088 (2020).
- 23. Yang, M., Ye, Z., Farhat, M. & Chen, P. Y. Enhanced radio-frequency sensors based on a self-dual emitter-absorber. *Phys. Rev. Appl.* 15, 014026 (2021).
- 24. Yang, M. et al. Electromagnetically unclonable functions generated by non-hermitian absorber-emitter. Sci. Adv. 9, 7481 (2023).
- 25. Zhi, Y. et al. Extraordinary characteristics for one-dimensional parity-time-symmetric periodic ring optical waveguide networks. *Photon. Res.* **6**, 579–586. https://doi.org/10.1364/PRJ.6.000579 (2018).
- Gyger, F. et al. Observation of stimulated brillouin scattering in silicon nitride integrated waveguides. *Phys. Rev. Lett.* 124, 013902. https://doi.org/10.1103/PhysRevLett.124.013902 (2020).
- 27. Luke, K., Okawachi, Y., Lamont, M. R., Gaeta, A. L. & Lipson, M. Broadband mid-infrared frequency comb generation in a Si_3 N_4 microresonator. Opt. Lett. 40, 4823–4826. https://doi.org/10.1364/OL.40.004823 (2015).
- 28. Wang, Z. Y. & Yang, X. B. Strong attenuation within the photonic band gaps of multiconnected networks. *Phys. Rev. B* 76, 235104. https://doi.org/10.1103/PhysRevB.76.235104 (2007).
- Zhang, Z. Q. et al. Observation of localized electromagnetic waves in three-dimensional networks of waveguides. *Phys. Rev. Lett.* 81, 5540. https://doi.org/10.1103/PhysRevLett.81.5540 (1998).
- 30. Lu, J., Yang, X. B. & Cai, L. Z. Large photonic band gap and strong attenuation of multiconnected peano network. *Opt. Commun.* 285, 459–464. https://doi.org/10.1016/j.optcom.2011.09.064 (2012).
- Markos, P. & Soukoulis, C. M. Wave Propagation: From Electrons to Photonic Crystals and Left-Handed Materials (Princeton University Press. 2008).
- 32. Kohmoto, M., Sutherland, B. & Iguchi, K. Localization of optics: Quasiperiodic media. *Phys. Rev. Lett.* 58, 2436–2438. https://doi.org/10.1103/PhysRevLett.58.2436 (1987).
- 33. Zhu, P. et al. Formation of photonic band gaps by direct destructive interference. Opt. Express 31, 43390-43400. https://doi.org/10.1364/QE.507977 (2023).
- Bender, C. M. & Boettcher, S. Real spectra in non-Hermitian Hamiltonians having PT symmetry. *Phys. Rev. Lett.* 80, 5243. https://doi.org/10.1103/PhysRevLett.80.5243 (1998).
- Wu, J. Y. & Yang, X. B. Ultrastrong extraordinary transmission and reflection in PT-symmetric Thue-Morse optical waveguide networks. Opt. Express 25, 27724–27735. https://doi.org/10.1364/OE.25.027724 (2017).
- 36. Wu, J. Y., Wu, X. H., Yang, X. B. & Li, H. Y. Extraordinary transmission and reflection in PT-symmetric two-segment-connected triangular optical waveguide networks with perfect and broken integer waveguide length ratios. *Chin. Phys. B* 28, 104208. https://doi.org/10.1088/1674-1056/ab3f92 (2019).
- Xu, J. F., Yang, X. B., Chen, H. H. & Lin, Z. H. Extraordinary propagation characteristics of electromagnetic waves in one-dimensional anti-PT-symmetric ring optical waveguide network. *Chin. Phys. B* 29, 064201. https://doi.org/10.1088/1674-1056/ab 8371 (2020).
- 38. Chen, H. H., Xu, J. F., Yang, X. B. & Lin, Z. H. Extraordinary optical characteristics of one-dimensional double anti-PT-symmetric ring optical waveguide networks, Chinese. *J. Phys.* 77, 816–825. https://doi.org/10.1016/j.cjph.2021.07.039 (2021).
- Longhi, S. Optical realization of relativistic non-Hermitian quantum mechanics. Phys. Rev. Lett. 105, 013903. https://doi.org/10.1 103/PhysRevLett.105.013903 (2010).

Acknowledgements

This work was supported by the National Natural Science Foundation of China, Grant Nos.: 11674107, 61475049, 11775083, 61774062, and 61771205.

Author contributions

Y.Z. and M.H. wrote the main manuscript text and prepared Figs. 1, 2, 3, 4, 5 and 6; X.Y. proposed the main research methods in the manuscript and reviewed the manuscript.

Declarations

Competing interests

The authors declare no competing interests.

Additional information

Correspondence and requests for materials should be addressed to X.Y.

Reprints and permissions information is available at www.nature.com/reprints.

Publisher's note Springer Nature remains neutral with regard to jurisdictional claims in published maps and institutional affiliations.

Open Access This article is licensed under a Creative Commons Attribution-NonCommercial-NoDerivatives 4.0 International License, which permits any non-commercial use, sharing, distribution and reproduction in any medium or format, as long as you give appropriate credit to the original author(s) and the source, provide a link to the Creative Commons licence, and indicate if you modified the licensed material. You do not have permission under this licence to share adapted material derived from this article or parts of it. The images or other third party material in this article are included in the article's Creative Commons licence, unless indicated otherwise in a credit line to the material. If material is not included in the article's Creative Commons licence and your intended use is not permitted by statutory regulation or exceeds the permitted use, you will need to obtain permission directly from the copyright holder. To view a copy of this licence, visit https://creativecommons.org/licenses/by-nc-nd/4.0/.

© The Author(s) 2024